International Journal of Chemical, Materials and Biomolecular Sciences
ISSN: 2415-6620
Vol:15, No:4, 2021

Comparative Study on the Effect of Substitution of Li and Mg Instead of Ca on Structural and Biological Behaviors of Silicate Bioactive Glass

Alireza Arab, Morteza Elsa, Amirhossein Moghanian

Abstract**—**In this study, experiments were carried out to achieve a promising multifunctional and modified silicate based bioactive glass (BG). The main aim of the study was investigating the effect of lithium (Li) and magnesium (Mg) substitution, on *in vitro* bioactivity of substituted-58S BG. Moreover, it is noteworthy to state that modified BGs were synthesized in $60SiO_2$–(36-x)CaO–$4P_2O_5$–(x)Li_2O and $60SiO_2$–(36-x)CaO–$4P_2O_5$–(x)MgO (where x = 0, 5, 10 mol.%) quaternary systems, by sol-gel method. Their performance was investigated through different aspects such as biocompatibility, antibacterial activity as well as their effect on alkaline phosphatase (ALP) activity, and proliferation of MC3T3 cells. The antibacterial efficiency was evaluated against methicillin-resistant *Staphylococcus aureus* bacteria. To do so, CaO was substituted with Li_2O and MgO up to 10 mol % in 58S-BGs and then samples were immersed in simulated body fluid up to 14 days and then, characterized by X-ray diffraction, Fourier transform infrared spectroscopy, inductively coupled plasma atomic emission spectrometry, and scanning electron microscopy. Results indicated that this modification led to a retarding effect on *in vitro* hydroxyapatite (HA) formation due to the lower supersaturation degree for nucleation of HA compared with 58s-BG. Meanwhile, magnesium revealed further pronounced effect. The 3-(4,5 dimethylthiazol-2-yl)-2,5 diphenyltetrazolium bromide (MTT) and ALP analysis illustrated that substitutions of both Li_2O and MgO, up to 5 mol %, had increasing effect on biocompatibility and stimulating proliferation of the pre-osteoblast MC3T3 cells in comparison to the control specimen. Regarding to bactericidal efficiency, the substitution of either Li or Mg for Ca in the 58s BG composition led to statistically significant difference in antibacterial behaviors of substituted-BGs. Meanwhile, the sample containing 5 mol % CaO/Li_2O substitution (BG-5L) was selected as a multifunctional biomaterial in bone repair/regeneration due to the improved biocompatibility, enhanced ALP activity and antibacterial efficiency among all of the synthesized L-BGs and M-BGs.

Keywords**—**Alkaline, alkaline earth, bioactivity, biomedical applications, sol-gel processes.

I. Introduction

BIOMATERIALS science is the filed which has had positive effect on humans health. Professor Hench et al. invented certain glass for the first time in the 1970s, which was capable of bonding directly to the host bone tissue by forming a HA interface layer on its surfaces after implantation [1]-[3]. BGs can be synthesized using melt-quenching or sol-gel methods [4]. The sol–gel method uses significant lower temperature which provides high purity in BG's composition with respect to the melt-quenching method [5]. Moreover, sol-gel derived BGs exhibit higher bioactivity due to their higher dissolution rate because of their higher specific surface area compared with melt-quench derived BGs [6].

Some studies reported the synthesis and characterization of 58S-BG (60% SiO_2-36% CaO-4% P_2O_5 (mol %) [6]-[8]. In addition, the improvement of BGs properties such as osteoconductivity [9], [10], angiogenicity [11] and antibacterial [12] can be obtained by modifying the BGs with various amounts of modifier such as alkaline [13], alkaline earth [14]-[17], transition [11], [18], [19] and post-transition elements [20].

Bacterial infection is a serious impediment to the utility of medical implants. Each year in US, approximately 4.3% inserted orthopedic implants become infected [21]. Despite sterilization and aseptic procedures, some pathogenic microorganisms are still present at approximately 90% of all implants. So, one of the intelligent alternatives to antibiotics or bactericidal agents in the treatment of infections such as *Staphylococcus aureus* is antibacterial BGs. *Staphylococcus aureus* is the most common bacterial and methicillin-resistant *Staphylococcus aureus* (MRSA), kind of staphylococcus resistant to the methicillin and other related antibiotics, is hospital-acquired infection and has been identified as a threat to human health [22].

Previous studies reveal that the presence of lithium (Li) and magnesium (Mg) in a BGs composition can enhance their therapeutic properties i.e., Li ions by either the promotion or inhibition of growth of osteoblast and osteoclast cells can enhance new bone formation [23], [24]. In addition, this ion can increase the proliferation of neural progenitor cells [25] and remyelination of peripheral nerves [26] as well as bone mass [27]. Moreover, lithium substituted BGs improve proliferation, differentiation, osteogenic activity of osteoblasts and cementogenic gene expression in mesenchymal stem cells (MSCs) [28], [29]. On the other hand, Magnesium (Mg) as a second most prevalent intracellular cation in the human body [21], [30], has a major role in the bone development and osteoporosis prevention due to increasing the osteoblast cell activity and inhibiting the osteoclast differentiation [31], [32]. Moreover, antibacterial activity of magnesium has been previously reported [33], [34]. As mentioned above, both of the lithium substituted (Li-BGs) and magnesium substituted BGs (Mg-BGs) exert nearly the same effect on *in vitro* HA formation, cells proliferation and activity as well as

Alireza Arab* and Morteza Elsa are with the Scientific and technology park, Imam Khomeini International University, Qazvin, 34149-16818, Iran (*Corresponding author, e-mail: alireza.arab.1996.bio@gmail.com).

Amirhossein Moghanian is with the Department of Materials Engineering, Imam Khomeini International University, Qazvin, 34149-16818, Iran.

bactericidal efficiency. Therefore, the main aims of this study were first to compare how *in vitro* bioactivity was affected by substitution of either Li^+ or Mg^{2+} with Ca in 58S-BG; and second, to introduce an optimal composition in Li- and Mg-substituted as a promising candidate in bone tissue engineering with increased cell proliferation, ALP activity, and more efficient antibacterial potential against MRSA bacteria compared to the BG-58s. For this purpose, at first, four sol-gel derived $60SiO_2$–(36-x)CaO–$4P_2O_5$–(x)Li_2O and $60SiO_2$–(36-x)CaO–$4P_2O_5$–(x)MgO quaternary systems (with x = 5, 10 mol %) were synthesized. Afterwards, X-ray diffraction (XRD), Fourier transform infrared (FT-IR), Inductively coupled plasma atomic emission spectrometry (ICP-AES) and scanning electron microscopy (SEM) were conducted to investigate the effect of Li_2O/CaO and MgO/CaO substitution on *in vitro* bioactivity.

In order to study the quantitative biological evaluation, MTT and ALP activity assays were performed to compare proliferation and differentiation of untreated MC3T3-E1cells compared to those treated with synthesized L-BGs and M-BGs. Furthermore, Live/Dead and DAPI/Actin staining fluorescent microscopy were used to assess cell viability qualitatively. eventually, according to the *in vitro* bioactivity, cell proliferation, ALP and antibacterial activity results, the optimal composition in $60SiO_2$–(36-x)CaO–$4P_2O_5$–(x)Li_2O and $60SiO_2$–(36-x)CaO–$4P_2O_5$–(x)MgO quaternary systems (with x = 5, 10 mol %) was reported.

II. Materials and Methods

A. BG Synthesis

Firstly, tetraethyl orthosilicate (TEOS) was dissolved in distilled water, and 0.1 M nitric acid for 1 h at room temperature on magnetic stirrer. After the complete hydrolysis of TEOS, triethyl phosphate (TEP) was added to the solution while stirring for 45 min. Then, calcium nitrate tetrahydrate $Ca(NO_3)_2.4H_2O$, and lithium nitrate ($LiNO_3$) or magnesium nitrate hexahydrate $Mg(NO_3)_2.6H_2O$ were consequently added to the obtained solution at 45 min intervals under constant stirring to obtain a transparent sol.

The resulting sol was aged at 37 °C for 3 days, drying at 75 °C for 24 h and calcinating at 700 °C for 3 h to eliminate the nitrates and organic substances. The obtained BG was then ground into a fine powder with particle size range below 50 µm using a zirconia planetary ball mill (Retsch, Germany). Moreover, for *in vitro* evaluations, 9 MPa pressure was applied to the BGs powder using a hydraulic press to form disc-shaped (Ø10×3 mm) samples. All the starting materials were purchased from Merck (KGaA, Germany) and used without further purification. Table I presents different elemental compositions of synthesized L-BGs and M-BGs.

B. Preparation of SBF

Simulated body fluid (SBF) solution with a similar chemical composition to the human plasma was prepared according to Kokubo's recipe by dissolving appropriate quantities of the relevant reagent-grade chemicals in deionized water [35].

Sodium sulfate (Na_2SO_4), sodium chloride (NaCl), potassium chloride (KCl), sodium bicarbonate ($NaHCO_3$), calcium chloride ($CaCl_2$), magnesium chloride hexahydrate ($MgCl_2{\cdot}6H_2O$), monopotassium phosphate (KH_2PO_4), tris hydroxymethyl aminomethane (Tris-buffer) and hydrochloric acid (HCl) were extra pure grade and were purchased from Merck KGaA, Germany. The comparison of prepared SBF composition with the human blood plasma is presented in Table II.

TABLE I
Elemental Composition of Synthesized BGs

BG	Label	SiO_2	CaO	P_2O_5	Li_2O	MgO
58s	BG-0	60	36	4	0	0
58s-5 mol % Li_2O	BG-5L	60	31	4	5	0
58s-5 mol % MgO	BG-5M	60	31	4	0	5
58s-10 mol % Li_2O	BG-10L	60	26	4	10	0
58s-10 mol % MgO	BG-10M	60	26	4	0	10

TABLE II
Oxygen Density Values of BGs

Ion	Plasma (mmol.L^{-1})	SBF (mmol.L^{-1})
Na^+	142.0	142.0
K^+	5.0	5.0
Mg^+	1.5	1.5
Ca^{+2}	2.5	2.5
Cl^-	103.0	147.8
HCO_3^-	27	4.2
HPO_4^{-2}	1.0	1.0
SO_4^{-2}	0.5	0.5

C. Characterization of Synthesized BGs

1. XRD Analysis

XRD (INEL-Equinox-3000, France) was conducted in order to evaluate the formation of HA on glass surfaces after 1 day, 3 days, 7 days and 14 days, with a Cu-Kα radiation source (λ =1.5405 A°) at 40 kV with 2Θ value varying from 20° to 50°.

2. FTIR Analysis

In vitro bioactivity was determined by analyzing the change of functional groups in the wavenumber range of 400–4000 cm^{-1} with a resolution of 8 cm^{-1} by FTIR spectroscopy (Nicolet Avatar 660, USA) using KBr pellet technique. The prepared sample each of 1 mg fine BG powder was mixed with 100 mg KBr (at the weight ratio of 1:100) in an agate mortar and pressed into a pellet.

3. SEM

SEM (Philips XL30, Netherland) was employed in order to observe the morphology of the BG disc's surface to monitor HA formation and its growth after 7 days and 14 days of immersion.

4. ICP-AES

The ionic exchanges study was performed by using ICP-AES (Varian Vista Pro, Palo Alto, USA). After 1 day, 3 days, 7 days and 14 days of immersion, the SBF solutions were analyzed for Ca, Si, P, Li and Mg ions.

C.5. pH measurement

The variations in pH of the SBF over immersion time up to 14 days was recorded by a calibrated pH meter (Corning pH meter 340, USA) at each step.

D. Biological Evaluation

1. Cell Culture

A mouse osteoblast-like cell line, MC3T3-E1, was cultured in a 50/50 α-minimal essential medium (αMEM)/Dulbecco's modified essential medium (DMEM) supplemented with 10% fetal bovine serum (FBS), 1% antibiotic, 0.1% penicillin-streptomycin and 2 mM glutamine at 37 °C in a humidified incubator containing 5% CO_2. The medium was changed every other day and confluent cells were subcultured by trypsinization. MC3T3-E1cells, medium and other supplements were purchased from (Sigma-Aldrich, Poole, UK).

2. Live-Dead Assay

The viability/cytotoxicity (Live-dead) assay (xxx Probes, UK) was performed according to the manufacturer's instructions to qualitatively assess cell viability and to determine whether L-BG and M-BG were cytotoxic [36]. Briefly, MC3T3-E1cells were cultured in the presence of BG-0 (as a control sample), BG-5L and BG-5M (as a peak samples in L-BGs and M-BGs with the highest cell proliferation based on MTT results) for 1 day and 7 days and followed by incubation with 4 mM ethidium homodimer-1 (EthD-1, Sigma, USA) and 2 mM calcein-acetoxymethyl ester (Calcein/AM, Sigma, USA). Stained cells (live cells: green stain, dead cells: red stain) were visualized using fluorescence microscope (Olympus, USA) and representative images were recorded.

3. Actin Staining of cells

After 1 day and 7 days of culture, Alexa Fluor-594 phalloidin (Invitrogen, CA, USA) and 4,6-diamidine-2-phenylindole (DAPI) solution (Invitrogen, CA, USA) were respectively applied in DAPI/Actin staining in order to visualize the cytoskeleton labeled in green fluorescence and nuclei of MC3T3-E1 cells labeled in blue fluorescence in presence of BG-0, BG-5L and BG-5M [37].

4. MTT Assay and ALP Analysis

MTT assay was conducted to measure cell viability after incubation with synthesized L-BGs and M-BGs powders by reduction of tetrazolium salt to formazan crystals by the mitochondria of viable cells [38].

The activity of ALP was evaluated by measuring the conversion of p-nitrophenyl phosphate to p-nitrophenol [39]. The procedure was performed according to the manufacturer's protocol (BioCat, Heidelberg, Germany). First, MC3T3-E1 cells at a density of 1×10^4 cells/cm^2 were cultured on BG-0, L-BGs and M-BGs for 1 day, 3 days and 7 days in a humid incubator at 37 °C and 5% CO_2. After each time period, the supernatant fluid pipette out and the cell layer was washed gently with PBS and followed by homogenizing in 1 ml Tris buffer and sonicated on ice for 4 min. Then, 20 µl of Aliquots were added to 1 ml of a p-nitrophenyl phosphate solution (pNPP, Sigma, 16 mM) and the activity of enzyme was quantized by absorbance at 410 nm after [40].

5. Bactericidal Studies

To evaluate the influence of Li and Mg on antibacterial activities in BG-58S against MRSA bacteria, the bactericidal activity of L-BGs and M-BGs was studied as previously described [41]. First, we diluted cultured MRSA in liquid lysogenybroth (LB) medium approximately to 0.5×10^8 to 2×10^8 ml^{-1} [41] then 0.1 ml bacterial suspension was added to a mixture of 0.9 ml LB medium and 10 mg BGs powder followed by stirring for 1 min and cultured for 1 h at 37 °C. Finally, cultured bacteria were diluted serially and 100 µl suspensions were plated onto LB-agar plates and incubated overnight at 37 °C in the dark [41]. After dilution serially, 100 µl suspensions were streaked onto LB-agar plates and incubated at 37 °C in the dark for 24 h [41].

Final colony-forming units per milliliter (CFU/ml) method was applied to calculate the bactericidal percentages by following formula as previously reported [41], [42]:

$$\text{Bactericidal fraction} = 1 - (\text{number of survived bacteria}/\text{number of total bacteria})$$

E. Statistical Analysis

The data expressed as the mean ± standard deviations (SD) between groups were determined by GraphPad Prism software package, version 3.0 (GraphPad Prism, USA) with values of *P < 0.05. (*p < 0.05, **p < 0.01, ***p < 0.001 and ****p < 0.0001). The elemental analysis and cell assays were performed with three independent experiments, each with triplicate samples.

III. Results and Discussion

A. Phase Analysis

Figs. 1 (a) and (b) show the XRD patterns of synthesized BGs after immersion for 7 days and 14 days in SBF solution. As seen in Fig. 1 (a), after 3-day immersion, XRD pattern of BG-0, and BG-5L exhibited tow peaks at 2Θ equal to 25.8° and 31.8° which attributed to (200) and (211), respectively and approved the formation of crystalline HA (HA; JCPDS 09-432) while, BG-10L and BG-5M showed one peak at 2Θ equal to 31.8°. Meanwhile, no characteristic peak was detected in XRD pattern of BG-10M. The mentioned peaks became more pronounced over immersion time up to day 14 because of the growth of formed crystalline HA. On day 14, the peak attributed to (200) plane at 2Θ equal to 25.8° was revealed for BG-5M and BG-10L. While, showed XRD pattern of BG-10M exhibited no characteristic peaks, Fig. 1 (b). The highest *in vitro* bioactivity of BG-0 was confirmed by detecting two new peaks at 2Θ equal to 32.18° (assigned to (112) plane) and 32.86° (assigned to (300) plane) after 14 days of immersion which affirmed the maturity of the formed crystalline HA [43].

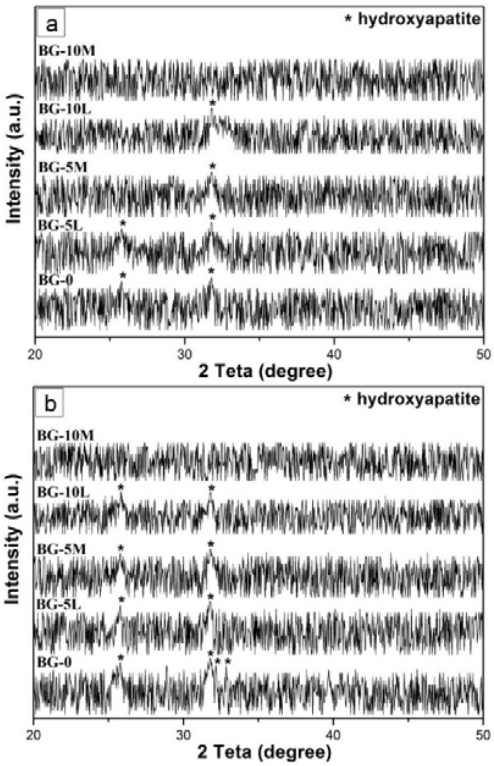

Fig. 1 The XRD patterns of BG-0, BG-5M, BG-5S, BG-10M and BG-10S after (a) 7 days and (b) 14 days of soaking in SBF

Khorami et al. suggested that the formation of HA layer on melt-derived lithium-modified 45S5 based glass was dose-dependent and decreased by increasing the Li [29]. Amjad et al. [44] and Roy et al. [45] previously reported that the substitution of Mg/Ca decreased the *in vitro* bioactivity by blocking the active calcium phosphate growth sites through adsorption of Mg^{2+} at the crystal surfaces which interpreted in terms of a Langmuir isotherm. Moreover, lower rate of HA formation on SiO_2–CaO–MgO–P_2O_5 BG with higher MgO content was observed by Ma et al. [46].

Taken together, XRD results revealed that substitution of both Li and Mg in BG composition in the range of 0 to 10 mol%, retarded the *in vitro* HA formation. In addition, BG-5L exhibited a nearly similar trend to BG-0 with slightly lower intensity. Meanwhile, magnesium had more pronounced effect on reduction of in vitro bioactivity with respect to the lithium.

B. Structural Groups

Figs. 2 (a) and (b) present FTIR spectra of all synthesized BGs after immersion in SBF for 7 days and 14 days. FTIR spectra of all BGs showed characteristic peaks attributed to Si–O–Si. The peaks near 470 cm^{-1}, 790 cm^{-1}, 1000–1100 cm^{-1} and 1250 cm^{-1} were due to bending vibration mode of Si–O–Si, symmetric stretching of Si–O, symmetric and asymmetric stretching of Si–O–Si, respectively [47]. Moreover, peaks appeared at 570 cm^{-1} and 603 cm^{-1} were due to the asymmetric bending mode of PO_4^{3-} group [48], [49] and the band located at 3500 cm^{-1} and 1651 cm^{-1} was related to symmetric stretching mode of the O–H [50]. Additionally, peaks observed near 870 cm^{-1} and 1455 cm^{-1} were assigned to C–O stretching in carbonate groups substituted for phosphate groups in HA lattice. Meanwhile, previous study reported that the vibration peaks at 566 cm^{-1}, 603 cm^{-1} and 1030–1090 cm^{-1} are characteristic of HA [51].

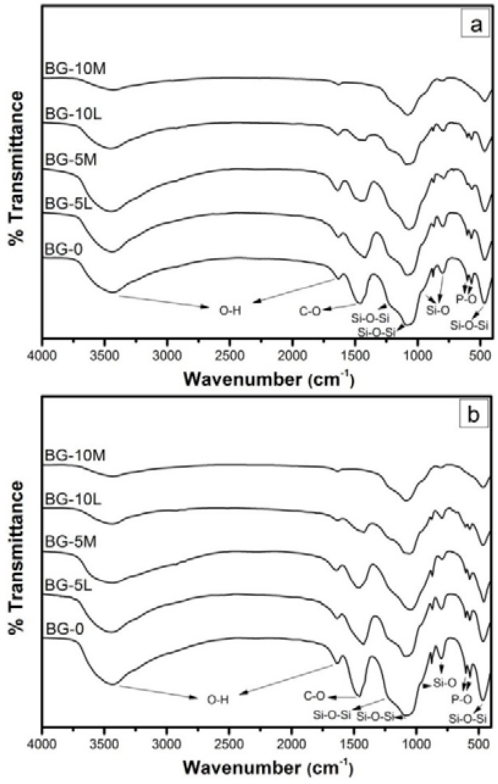

Fig. 2 FTIR spectra of BG-0, BG-5L, BG-5M, BG-10L and BG-10M after 7 days and 14 days of soaking in SBF

As seen in Fig. 2 (a), after 7 days of immersion, the appearance of a split phosphate peaks, indicative of the formation of calcium phosphate, was detected at 570 cm^{-1} and 603 cm^{-1} in BG-0 FTIR spectrum. Similarly, BG-5L, BG-10L and BG-5M revealed P–O bending bands on day 7, while BG-10M did not observe these bands. Meanwhile, BG-0 exhibited a higher intensity and the order of intensity for the mentioned peaks was: BG-0 > BG-5L > BG-10L > BG-5M. With increasing the immersion time to 14 days, both P–O and C–O bands were enhanced in intensity. On the other hand, FTIR spectra of the BG-10M showed no detectable P–O and C–O bands after14 days immersion in SBF which was in good agreement with XRD results that confirmed HCA formation on surfaces of the BG-0, BG-5L, BG-5M after immersion for 7 days in SBF solution.

Altogether, FTIR results revealed that substitution the low amount of Li (5 mol %) in BG-58S (BG-5L) had not significant effect on *in vitro* HA formation and the retarding effect of Mg was more pronounced compared with Li. Meanwhile, BG-10M exhibited the lowest bioactivity among other BGs due to no P–O and C–O bands detection in its FTIR

spectrum even on day 14 of immersion.

C. Ion Chemistry of SBF Solution

The dissolution/precipitation of ions from the BG surface and SBF solution during the crystallization of HA leads to variation the concentration of the Ca, Si and P ions and results in variation the pH of the SBF solution [52]. The changes in concentration of Ca, Si, P, Li and Mg concentration in the SBF solution and pH values for different immersion time up to 14 days are presented in Figs. 3 (a)-(f).

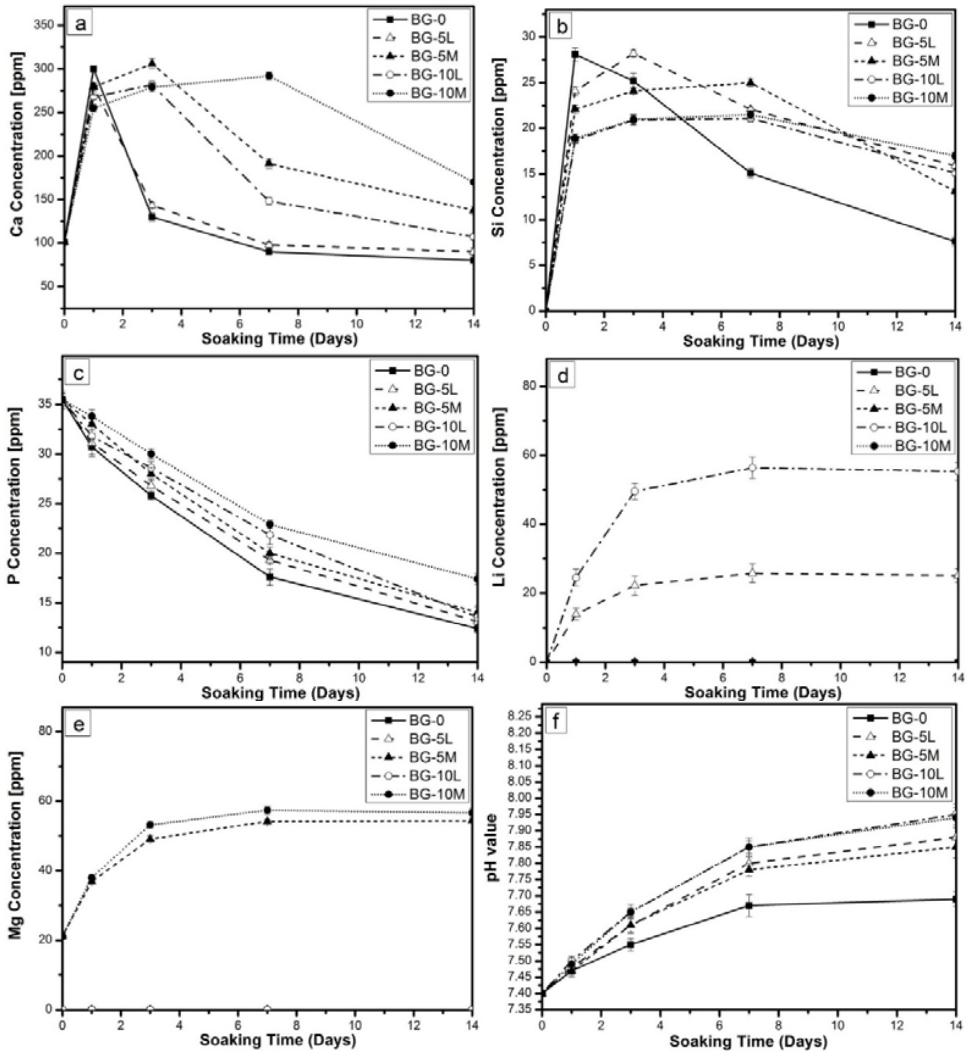

Fig. 3 Calcium (a), silicon (b), phosphorus (c), lithium (d), magnesium (e) ions concentrations in the SBF solution monitored over immersion time (f) PH values in different soaking times

Fig. 3 (a) demonstrates that Ca concentrations [Ca] in SBF solution for BG-0, BG-5L, BG-5M, BG-10L and BG-10M increased significantly from 100 $mg.L^{-1}$ in the SBF solution to 300.4 $mg.L^{-1}$, 280.1 $mg.L^{-1}$, 279.3 $mg.L^{-1}$, 267.7 $mg.L^{-1}$ and 255 $mg.L^{-1}$ after 1 day of immersion, respectively. By increasing the immersion time to day 3, [Ca] values decreased for BG-0 to about 130.1 indicating the substantial rate of precipitation of calcium phosphate compounds while, for and BG-5L, BG-5M, BG-10L and BG-10M, [Ca] gradually increased to day 3 of immersion. On day 3, [Ca] decreased for BG-5L to around 143.2 $mg.L^{-1}$ while, [Ca] for other BGs slightly increased until day 7 and then decreased at a lower rate with respect to BG-0 and BG-5L. Meanwhile, BG-10M had the lowest decreasing rate of [Ca] among all other BGs.

Si concentrations [Si] with nearly similar trend like [Ca], were decreased by the substitution of Li and Mg for Ca in the BG's compositions (Fig. 3 (b)). The BG-0 showed a decrease in [Si] on day 3, while, this occurred on day 7 for BG-5L and on day 14 for BG-5M, BG-10L and BG-10M. In other words, substitution of Ca with Li and Mg ions in BG decreased the L-BGs and M-BGs solubility by increasing the field strength of Li^{+} and Mg^{2+} ions compared to Ca^{2+} due to the smaller ionic radius of Li^{+} and Mg^{2+} compared to Ca^{2+} (Li^{+}, Mg^{2+}, Ca^{2+} : 76 ppm, 72 ppm, 100 ppm [53]-[55]) which led to a higher

oxygen density of the L-BGs and M-BGs compared to the BG-0. Therefore, the main possible reason for the lower bioactivity of L-BGs and M-BGs was lower supersaturation degree and driving force for HA nucleation due to their higher field strength and structures compactness compared with BG-0 which prevented easy cationic exchange by inhibiting the penetration of SBF solution inside the substituted BGs structure.

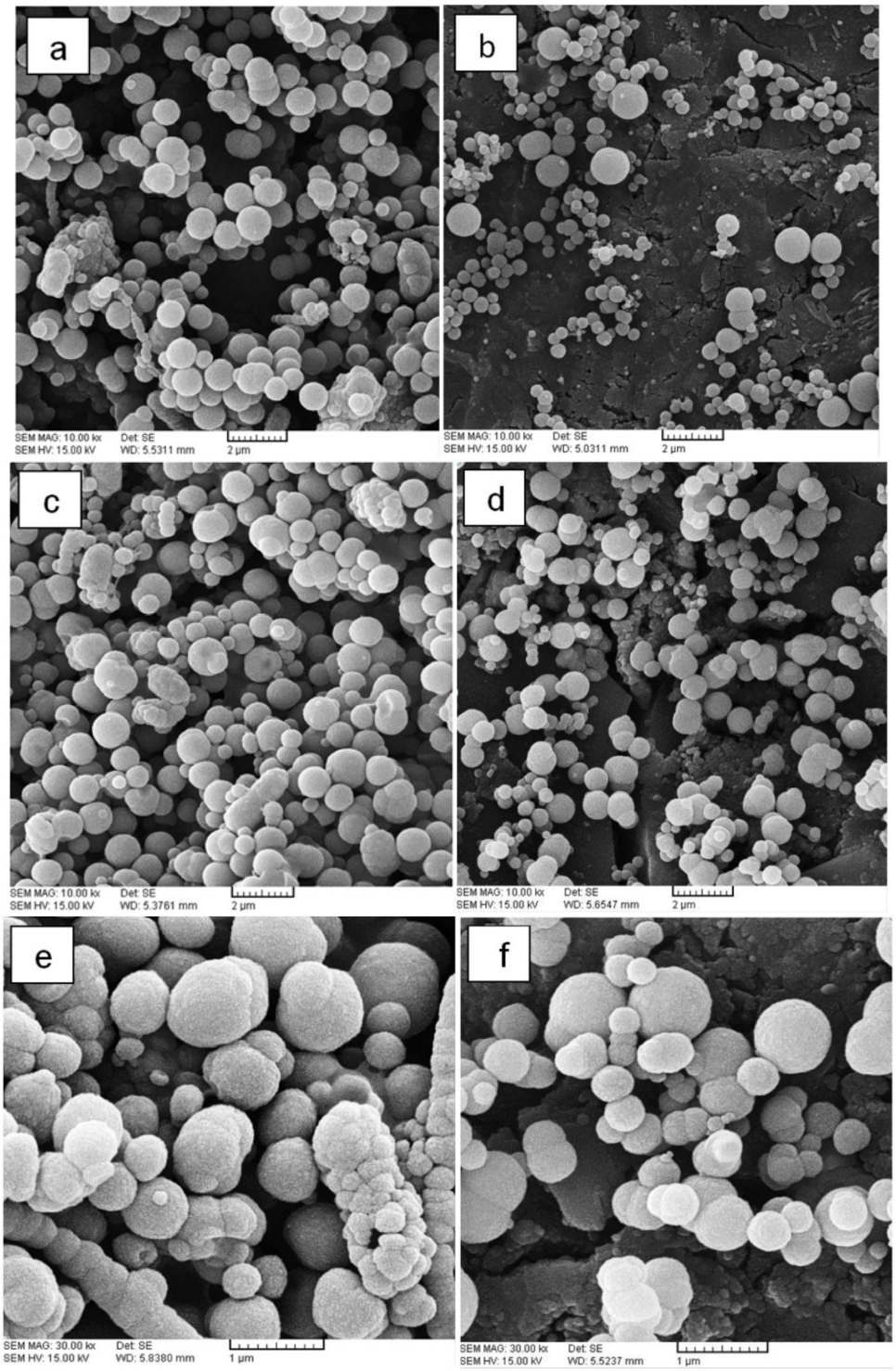

Fig. 4 SEM images of BG-5M ((a) and (c) (higher magnification)) and BG-5S ((b) and (d) (higher magnification)) after 14 days of immersion in the SBF solution

By neglecting the dissolution of P from the BGs, the P concentration [P] in the SBF is used to make an estimate to compare the rate of HA precipitation [13]. According to Fig. 3 (c), [P] decreased in L-BGs and M-BGs in comparison with BG-0 which confirmed a decrease in precipitation rate of HA formation in substituted BGs.

Figs. 3 (d) and (e) show the variation of Li concentration [Li] and Mg concentration [Mg] over immersion time. As it seen, Li and Mg releases in the SBF solution were higher in both L-BG and M-BG with more substitution (10 mol. %) with respect to BG-5L and BG-5M. Meanwhile, all of the synthesized L-BGs and M-BGs exhibited a rapid increase in [Li] and [Mg], respectively and reached a plateau on day 7 due to silica rich and HA layers formation on their surfaces and inhibition of cationic exchange between ions from the substituted BGs and H^+ from SBF [55], [56].

Fig. 3 (f) indicates the variations of pH values in the SBF solution over immersion time up to 14 days. According to Fig. 4 (f), the initial pH values increased rapidly from 7.4 until day 7 and then increased at a slower rate up to day 14. The first rapid increase in pH level was due to rapid cationic exchange between Ca^{+2}, Li^{+}, Mg^{+2} and H^+ and presence of more alkaline and alkaline earth ions in the SBF solution was led to the higher pH values. By increasing the immersion time, the increasing rate of pH values decreased because of a decrease in [Ca] due to HA formation [48].

D. Surface Microstructures

Figs. 4 (a)-(f) show the morphology of the formed HA on the surface of the BG-5L and BG-5M (with the highest bioactivity in L-BGs and M-BGs according to XRD and FTIR results) after immersion for 7 days and 14 days in SBF solution. As it was observed in Figs. 4 (a) and (b), after 7 days of immersion, HA nuclei were grown and the surfaces of BG-5L and BG-5M were partially covered by aggregates of formed HA. Meanwhile, BG-5L showed higher *in vitro* bioactivity by more aggregation of HA particles compared with BG-5M. On day 14, by comparison of Figs. 4 (c) and (d), it could be observed that HA had greater agglomeration compared to day 7 and surface of BG-5L was covered with more agglomerate than BG-5M.

Taken together, SEM observation suggested that BG-5L exhibited a promising HA formation ability after 7 days of immersion in SBF and it was in good agreement with XRD, FTIR and ICP-AES results which described in previous sections.

E. In vitro Biological Evaluation

1. Cell Proliferation

The proliferation of the cultured MC3T3-E1 osteoblastic cells on BG-0, L-BGs and M-BGs after 1 day, 3 days and 7 days is shown in Fig. 5. As it seen, at day 1, except BG-10M, slight increase was found in formation of formazan between the control and other BGs. By increasing the culture time, all the BGs exhibited an increase in their cell proliferation at 3 days and 7 days respect to the day one ($^*P < 0.01$) while, in each culture time, L-BGs and BG-10M respectively showed the highest and lowest MC3T3-E1 cells proliferation in comparison with control and BG-0. Meanwhile, there was no statistically significant difference between BG-5L and BG-10L in their optical density (OD) values ($^*P > 0.05$). According to Fig. 5, MC3T3-E1 cells were not only capable of growth over culture time up to 7 days in the presence of L-BGs, but also demonstrated a significant improvement in cell proliferation. Moreover, previous reports reveal the positive effect of both Li [29] and Mg [57] on the cells proliferation.

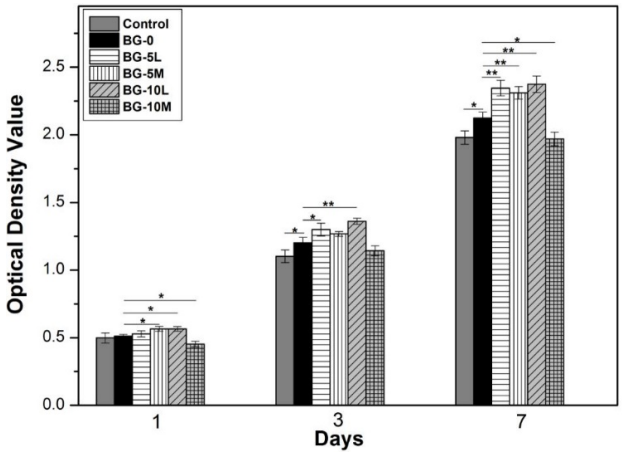

Fig. 5 Osteoblast-like cell line proliferation (MC3T3-E1), cultured on the synthesized BGs for 1 day, 3 days and 7 days (*p < 0.05 and **p < 0.01)

MTT results suggested that substitution of Li in range of 0 to 10 mol % in 58S BG composition was dose-independent and significantly enhanced the cell proliferation, while substitution of Mg was dose-independent, i.e. moderate amount of substitution (5 mol %) led to a significant increase of OD values while, more substitution (10 mol %) had reverse effect and significantly inhibited the MC3T3 cell proliferation.

2. ALP Activity

Fig. 6 shows the ALP activity of osteoblast-like cell line MC3T3-E1, cultured on synthesized BG-0, L-BGs and M-BGs for different culture times up to 7 day. As it seen from Fig. 6, a significant increase in ALP activity of all of the BGs from day 1 to day 7 of culture was observed. In other words, by increasing the culture time from 1 day to 7 days, the ALP activity enhanced around four times compared to day 1.

The positive effect of Li^+ ions on increasing the ALP activity of osteoblastic cells treated by lithium substituted 45S5 BGs was reported by [29]. Moreover, [28] suggested that substitution of 5% Li ions into mesoporous BG scaffolds improved its ALP level. Overall, all of the synthesized BGs except BG-10M exhibited the higher ALP level compared to the BG-0 at each culture time. Furthermore, the highest ALP activity was detected for BG-5L and BG-10L after culture for 7 days with no statistically significant difference between them ($^*P > 0.05$). Meanwhile, L-BGs had higher ALP levels than M-BGs.

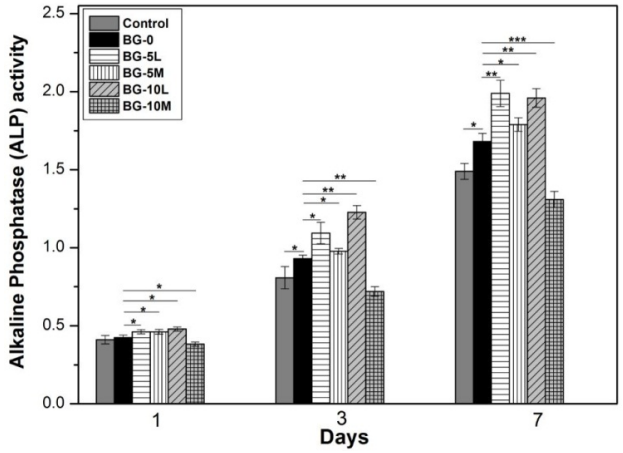

Fig. 6 ALP activities of osteoblast-like cell line (MC3T3-E1) cultured on synthesized BGs for 1 day, 3 days and 7 days (*p < 0.05 and **p < 0.01)

According to the XRD, FTIR, MTT and ALP results, BG-5L and BG-5M had the higher *in vitro* bioactivity, proliferation and osteoblastic activity of the MC3T3-E1 cells in synthesized L-BGs and M-BGs, respectively. So, in this research, BG-5L and BG-5M were selected as a peak samples for comparison with the control for Live-dead and DAPI/Actin staining assays.

3. Live-Dead Assay

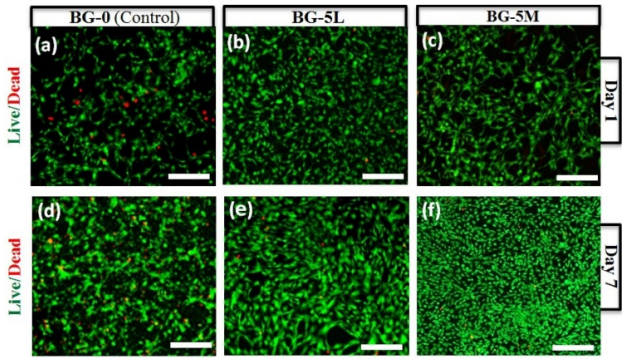

Fig. 7. Two-dimensional (2D) MC-3T3 cells cultured in presence of BG-0, BG-5M and BG-5S. Representative live/dead fluorescence images of MC-3T3 cells cultured on BG-0 (a, d), BG-5M (b, e) and BG-5S (c, f) after 1 day and 7 days of culture respectively. Green fluorescent cells are alive and red Fluorescent cells indicate dead cells. Scale bar represents 100 µm in all images

Figs. 7 (a)-(e) present the fluorescence staining of live and dead MC3T3 cells on BG-5L and BG-5M samples after 1 day and 7 days of culture. As it seen after one day in culture, the representative live/dead fluorescence images revealed that the MC3T3 cells treated by BG-5L and BG-5M had fewer dead cells (red staining) with respect to the BG-0 (as a control). By increasing the culture time to 7 days, cellular aggregates with different confluence were observed for cells treated with all of the BGs. Meanwhile, less proliferation were observed for BG-0 compared to BG-5L and BG-5M which confirmed by more dead cells in the live/dead fluorescent staining. Previous reports suggested that the cells biological response was influenced by various ions dissolution from BGs in culture medium [58]. Furthermore, pH variation is the other factor that affects the metabolic activity of osteoblasts [59].

Taken together, according to the live/dead staining observation, it could be suggested that BG-5L and BG-5M showed better cell proliferation due to a moderate concentration of released Li and Mg ions in culture medium and their related pH values between 7.4 and 7.85 (Fig. 3 (f)).

4. F-Actin Cytoskeleton

Figs. 8 (a)-(e) represent F-actin-labeled cytoskeleton of MC3T3 cells in presence of BG-0, BG-5L and BG-5M. As seen, F-actin fibers in green and nuclei in blue were arranged randomly with spindle-like elongated shape. This shape and orientation of F-actin fibers were reported by [60] in rat bone mesenchymal stem cells (rMSCs) treated by calcium carbonate ceramics. DAPI/Actin staining assay revealed that the mean number of DAPI-labelled nuclei for BG-5L and BG-5M were increased significantly over cuture time from 1 to 7 days. Meanwhile, MC3T3 cells treated with BG-5L and BG-5M had more DAPI-labelled nuclei with respect to the BG-0 which was indicative of good cytocompatibility of BG-5L and BG-5M. Consequently, Live-dead and Dapi/Actin assays confirmed that substituted 58s BG with moderate amount (5 mol %) of Li and Mg led to the better cell viability and proliferation compared to the Li or Mg free 58s BG which was in a good accordance with MTT results (Fig. 5).

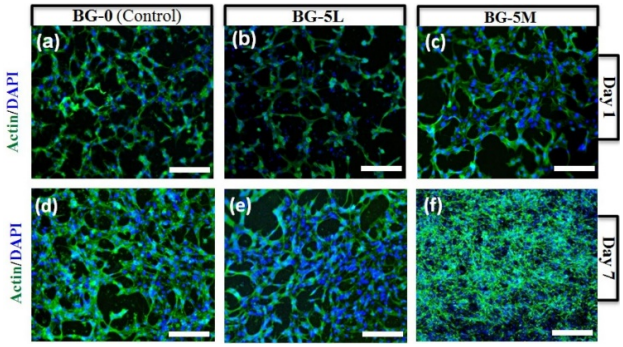

Fig. 8 Two-dimensional (2D) MC-3T3 cells cultured in presence of BG-0, BG-5 and BG-10. Representative ACTIN/DAPI fluorescence images of MC-3T3 cells cultured on BG-0 (a, d), BG-5L (b, e) and BG-5M (c, f) after 1 day and 7 days of culture respectively. Cell filaments are stained by Actin (green) and nuclei stained by DAPI (blue). Scale bar represents 100 µm in all images

5. Antibacterial Studies

Fig. 9 shows the antibacterial activity of synthesized BG-0, L-BGs and M-BGs against MRSA bacteria. From Fig. 9, it could be found that despite BG-10M, other synthesized L-BGs and BG-5M had bactericidal efficiency against MRSA at concentration of 0.01 g mL^{-1} compared to BG-0. In other words, there was no statistically significant difference in bactericidal efficiency between BG-10M and BG-0 ($^{*}P > 0.05$) while, BG-5L, BG-5M and BG-10L showed increased

antibacterial activity against MRSA bacteria. Meanwhile, BG-5L sample exhibited statistically higher significance antibacterial efficiency among all of the synthesized L-BGs and M-BGs in comparison with BG-0 ($^{***}p < 0.001$).

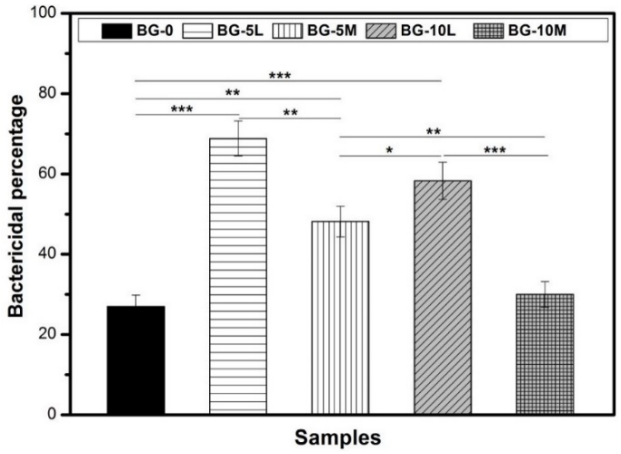

Fig. 9 The bactericidal percentages of 10 mg/mL of BG-0 (control), BG-5M, BG-5S, BG-10M and BG-10S. (*p < 0.05, **p < 0.01, ***p < 0.001 and ****p < 0.0001)

Albeit the exact mechanism of bactericidal activity of BGs is not yet clarified [61], but an increase in pH value of medium due to release of alkali ions as well as an inherent toxic effect of calcium, phosphate [61], lithium [62] and magnesium [34] from BGs are possible reasons for antibacterial activity of BGs [63], [64].

Results revealed that substitution of Li and Mg in the range of 0 to 10 mol % in L-BGs and M-BGs exhibited dose-independent and dose-dependent antibacterial activity against MRSA bacteria, respectively, i.e. both BG-5L and BG-10L showed statistically significant increase in antibacterial activity with respect to the BG-0. Meanwhile, there was no statistically significant difference between BG-5L and BG-10L (*P > 0.05). But, by 5 mol. % substitution of Mg in 58s BG, bactericidal efficiency increased significantly ($^{**}p < 0.01$) while, 10 mol.% substitution had no significant effect on bactericidal efficiency compared to BG-0 ($^{*}p < 0.05$). Taken together, BG-5L was presented as the most effective substituted BG against MRSA.

IV. Conclusion

In this research, the quaternary lithium and magnesium substituted BGs (in the range of 0 to 10 mol%) were successfully synthesized through the sol-gel method and the effects of Li and Mg substitution on BG-58s properties such as *in vitro* bioactivity, MC3T3 cells proliferation and activity as well as antibacterial efficiency were investigated and the following conclusions were drawn:

(i) The *in vitro* bioactivity was retarded by substitution of Li and Mg instead of Ca in BG composition and Mg had more pronounced effect with respect to the lithium.

(ii) ICP-AES results confirmed that solubility of the L-BGs and M-BGs decreased with respect to BG-0 because of increasing the field strength of Li^+ and Mg^{2+} ions compared to Ca^{2+} due to the smaller ionic radius of Li^+ and Mg^{2+} in comparison with Ca^{2+} which led to their higher oxygen density.

(iii) The detection of characteristic peaks of crystalline HA in XRD pattern as well as the appearance of C–O and P–O bands in FTIR spectra revealed that 58S-BG incorporating 5 mol% Li_2O in the composition (BG-5L) had nearly similar *in vitro* bioactivity to BG-0 while, BG-10M had the lowest *in vitro* HA formation.

(iv) MTT assay results showed that both 5 and 10 mol% Li_2O substitution (BG-5L, BG-10L) enhanced the MC3T3 cells proliferation and activity while 10 mol% Mg substitution led to statistically significant decrease in proliferation and activity of MC3T3 treated with BG-10M.

(v) Moderate (5 mol. %) substitution of both Li and Mg in 58S BG resulted in statistically significant increase in bactericidal efficiency against MRSA bacteria. Meanwhile, BG-5L exhibited the highest antibacterial activity among other BGs.

(vi) Taken together, by considering the *in vitro* bioactivity, biological evaluations such as cell proliferation and activity as well as antibacterial study, the sample BG-5L is presented as a promising candidate for in bone regeneration and tissue engineering applications with enhanced cell proliferation and promoted osteoblasts differentiation as well as antibacterial efficiency against MRSA bacteria.

References

[1] F. Gervaso, A. Sannino, G.M. Peretti, The biomaterialist's task: scaffold biomaterials and fabrication technologies, Joints, 1 (2013) 130.

[2] M. Tahriri, M. Del Monico, A. Moghanian, M.T. Yaraki, R. Torres, A. Yadegari, L. Tayebi, Graphene and its derivatives: Opportunities and challenges in dentistry, Materials Science and Engineering: C, 102 (2019) 171-185.

[3] M.P. Nikolova, M.S. Chavali, Recent advances in biomaterials for 3D scaffolds: A review, Bioactive materials, 4 (2019) 271-292.

[4] M. Kazem-Rostami, A. Moghanian, Hünlich base derivatives as photo-responsive Λ-shaped hinges, Organic Chemistry Frontiers, 4 (2017) 224-228.

[5] [5] M. Mozafari, F. Moztarzadeh, M. Rabiee, M. Azami, N. Nezafati, Z. Moztarzadeh, M. Tahriri, Development of 3D bioactive nanocomposite scaffolds made from gelatin and nano bioactive glass for biomedical applications, Advanced Composites Letters, 19 (2010).

[6] X. Zhang, Y. Yu, D. Jiang, Y. Jiao, Y. Wu, Z. Peng, J. Zhou, J. Wu, Z. Dong, Synthesis and characterization of a bi-functional hydroxyapatite/Cu-doped TiO2 composite coating, Ceramics International, 45 (2019) 6693-6701.

[7] A. Moghanian, F. Sharifianjazi, P. Abachi, E. Sadeghi, H. Jafarikhorami, A. Sedghi, Production and properties of Cu/TiO2 nano-composites, Journal of Alloys and Compounds, 698 (2017) 518-524.

[8] F. Shojaeepour, P. Abachi, K. Purazrang, A.H. Moghanian, Production and properties of Cu/Cr2O3 nano-composites, Powder technology, 222 (2012) 80-84.

[9] E. Kalantari, S.M. Naghib, N.J. Iravani, R. Esmaeili, M.R. Naimi-Jamal, M. Mozafari, Biocomposites based on hydroxyapatite matrix reinforced with nanostructured monticellite (CaMgSiO4) for biomedical application: synthesis, characterization, and biological studies, Materials Science and Engineering: C, 105 (2019) 109912.

[10] H. Shin, S. Jo, A.G. Mikos, Biomimetic materials for tissue engineering, Biomaterials, 24 (2003) 4353-4364.

[11] P.X. Ma, Biomimetic materials for tissue engineering, Advanced drug delivery reviews, 60 (2008) 184-198.

[12] M. Touri, F. Kabirian, M. Saadati, S. Ramakrishna, M. Mozafari, Additive manufacturing of biomaterials− the evolution of rapid prototyping, Advanced Engineering Materials, 21 (2019) 1800511.
[13] S. Kargozar, F. Baino, S. Hamzehlou, M.R. Hamblin, M. Mozafari, Nanotechnology for angiogenesis: opportunities and challenges, Chemical Society Reviews, 49 (2020) 5008-5057.
[14] A.J. Hassiba, M.E. El Zowalaty, G.K. Nasrallah, T.J. Webster, A.S. Luyt, A.M. Abdullah, A.A. Elzatahry, Review of recent research on biomedical applications of electrospun polymer nanofibers for improved wound healing, Nanomedicine, 11 (2016) 715-737.
[15] S. Chen, B. Liu, M.A. Carlson, A.F. Gombart, D.A. Reilly, J. Xie, Recent advances in electrospun nanofibers for wound healing, Nanomedicine, 12 (2017) 1335-1352.
[16] D. Khorsandi, A. Moghanian, R. Nazari, G. Arabzadeh, S. Borhani, Personalized Medicine: Regulation of Genes in Human Skin Ageing, J Allergy Ther, 7 (2016) 2.
[17] M. Norouzi, S.M. Boroujeni, N. Omidvarkordshouli, M. Soleimani, Advances in skin regeneration: application of electrospun scaffolds, Advanced healthcare materials, 4 (2015) 1114-1133.
[18] G. Suarato, R. Bertorelli, A. Athanassiou, Borrowing from Nature: biopolymers and biocomposites as smart wound care materials, Frontiers in bioengineering and biotechnology, 6 (2018) 137.
[19] S. Kargozar, F. Baino, S. Hamzehlou, R.G. Hill, M. Mozafari, Bioactive glasses entering the mainstream, Drug discovery today, 23 (2018) 1700-1704.
[20] J. Yang, T. Long, N.-F. He, Y.-P. Guo, Z.-A. Zhu, Q.-F. Ke, Fabrication of a chitosan/bioglass three-dimensional porous scaffold for bone tissue engineering applications, Journal of Materials Chemistry B, 2 (2014) 6611-6618.
[21] E. Pazos-Ortiz, J.H. Roque-Ruiz, E.A. Hinojos-Márquez, J. López-Esparza, A. Donohué-Cornejo, J.C. Cuevas-González, L.F. Espinosa-Cristóbal, S.Y. Reyes-López, Dose-dependent antimicrobial activity of silver nanoparticles on polycaprolactone fibers against gram-positive and gram-negative bacteria, Journal of Nanomaterials, 2017 (2017).
[22] M. Hosseinnejad, S.M. Jafari, Evaluation of different factors affecting antimicrobial properties of chitosan, International journal of biological macromolecules, 85 (2016) 467-475.
[23] K. Kalantari, A.M. Afifi, H. Jahangirian, T.J. Webster, Biomedical applications of chitosan electrospun nanofibers as a green polymer–Review, Carbohydrate polymers, 207 (2019) 588-600.
[24] R.C. Goy, D.d. Britto, O.B. Assis, A review of the antimicrobial activity of chitosan, Polímeros, 19 (2009) 241-247.
[25] K. Vimala, Y.M. Mohan, K.S. Sivudu, K. Varaprasad, S. Ravindra, N.N. Reddy, Y. Padma, B. Sreedhar, K. MohanaRaju, Fabrication of porous chitosan films impregnated with silver nanoparticles: a facile approach for superior antibacterial application, Colloids and Surfaces B: Biointerfaces, 76 (2010) 248-258.
[26] S. Kumar-Krishnan, E. Prokhorov, M. Hernández-Iturriaga, J.D. Mota-Morales, M. Vázquez-Lepe, Y. Kovalenko, I.C. Sanchez, G. Luna-Bárcenas, Chitosan/silver nanocomposites: Synergistic antibacterial action of silver nanoparticles and silver ions, European Polymer Journal, 67 (2015) 242-251.
[27] N. Nezafati, F. Moztarzadeh, S. Hesaraki, Z. Moztarzadeh, M. Mozafari, Biological response of a recently developed nanocomposite based on calcium phosphate cement and sol–gel derived bioactive glass fibers as substitution of bone tissues, Ceramics International, 39 (2013) 289-297.
[28] M. Aminitabar, M. Amirhosseinian, M. Elsa, Synthesis and in vitro Characterization of a Gel-Derived SiO2-CaO-P2O5-SrO-Li2O Bioactive Glass, International Journal of Chemical and Molecular Engineering, 13 (2019) 296-307.
[29] A. Pazhouheshgar, S.A.S. Vanini, A. Moghanian, The experimental and numerical study of fracture behavior of 58s bioactive glass/polysulfone composite using the extended finite elements method, Materials Research Express, 6 (2019) 095208.
[30] M. Elsa, A. Moghanian, Comparative Study of Calcium Content on in vitro Biological and Antibacterial Properties of Silicon-Based Bioglass, International Journal of Chemical and Molecular Engineering, 13 (2019) 288-295.
[31] A. Moghanian, S. Firoozi, M. Tahriri, A. Sedghi, A comparative study on the *in vitro* formation of hydroxyapatite, cytotoxicity and antibacterial activity of 58S bioactive glass substituted by Li and Sr, Materials Science and Engineering: C, 91 (2018) 349-360.
[32] A. Moghanian, A. Sedghi, A. Ghorbanoghli, E. Salari, The effect of magnesium content on *in vitro* bioactivity, biological behavior and antibacterial activity of sol–gel derived 58S bioactive glass, Ceramics international, 44 (2018) 9422-9432.
[33] A. Moghanian, S. Firoozi, M. Tahriri, Characterization, in vitro bioactivity and biological studies of sol-gel synthesized SrO substituted 58S bioactive glass, Ceramics International, 43 (2017) 14880-14890.
[34] A. Moghanian, S. Firoozi, M. Tahriri, Synthesis and *in vitro* studies of sol-gel derived lithium substituted 58S bioactive glass, Ceramics International, 43 (2017) 12835-12843.
[35] A. Moghanian, A. Ghorbanoghli, M. Kazem-Rostami, A. Pazhouheshgar, E. Salari, M. Saghafi Yazdi, T. Alimardani, H. Jahani, F. Sharifian Jazi, M. Tahriri, Novel antibacterial Cu/Mg-substituted 58S-bioglass: Synthesis, characterization and investigation of in vitro bioactivity, International Journal of Applied Glass Science, (2019).
[36] A. Moghanian, M. Zohourfazeli, M.H.M. Tajer, The effect of zirconium content on *in vitro* bioactivity, biological behavior and antibacterial activity of sol-gel derived 58S bioactive glass, Journal of Non-Crystalline Solids, 546 (2020) 120262.
[37] Z. Hajifathali, M. Amirhosseinian, The Effect of Substitution of CaO/MgO and CaO/SrO on *in vitro* Bioactivity of Sol-Gel Derived Bioactive Glass, International Journal of Biomedical and Biological Engineering, 13 (2019) 279-287.
[38] A. Moghanian, M. Zohourfazeli, Comparative study on *in vitro*, physico-chemical and antibacterial properties of 58S and 68S bioactive glasses synthesized by sol-gel method, 13 (2020) 17-30.
[39] S. Kargozar, F. Baino, S. Hamzehlou, R.G. Hill, M. Mozafari, Bioactive glasses: sprouting angiogenesis in tissue engineering, Trends in biotechnology, 36 (2018) 430-444.
[40] N. Nezafati, F. Moztarzadeh, S. Hesaraki, M. Mozafari, Synergistically reinforcement of a self-setting calcium phosphate cement with bioactive glass fibers, Ceramics International, 37 (2011) 927-934.
[41] M. Mozafari, F. Moztarzadeh, Synthesis, characterization and biocompatibility evaluation of sol–gel derived bioactive glass scaffolds prepared by freeze casting method, Ceramics International, 40 (2014) 5349-5355.
[42] M. Zohourfazeli, M.H.M. Tajer, A. Moghanian, Comprehensive investigation on multifunctional properties of zirconium and silver co-substituted 58S bioactive glass, Ceramics International, (2020).
[43] A. Moghanian, M. Zohourfazeli, Investigation the *In Vitro* and Bactericidal Properties of Magnesium and Copper Containing Bioactive Glasses, Journal of Advanced Materials and Technologies, 9 (2020) 19-33.
[44] A. Pazhouheshgar, A. Moghanian, S.A. Sadough Vanini, The Extended Finite Element Method Numerical and Experimental Analysis of Mechanical Behavior of Polysulfone/58s Bioactive Glass Synthesized through Solvent Casting Method, Modares Mechanical Engineering, 20 (2020) 2061-2073.
[45] S. Kargozar, F. Baino, S. Banijamali, M. Mozafari, Synthesis and physico-chemical characterization of fluoride (F)-and silver (Ag)-substituted sol-gel mesoporous bioactive glasses, Biomedical Glasses, 5 (2019) 185-192.
[46] H. Hu, Y. Tang, L. Pang, C. Lin, W. Huang, D. Wang, W. Jia, Angiogenesis and full-thickness wound healing efficiency of a copper-doped borate bioactive glass/poly (lactic-co-glycolic acid) dressing loaded with vitamin E *in vivo* and *in vitro*, ACS applied materials & interfaces, 10 (2018) 22939-22950.
[47] D. Moura, M. Souza, L. Liverani, G. Rella, G. Luz, J. Mano, A. Boccaccini, Development of a bioactive glass-polymer composite for wound healing applications, Materials Science and Engineering: C, 76 (2017) 224-232.
[48] S. Pourshahrestani, E. Zeimaran, N.A. Kadri, N. Gargiulo, H.M. Jindal, S.V. Naveen, S.D. Sekaran, T. Kamarul, M.R. Towler, Potency and cytotoxicity of a novel gallium-containing mesoporous bioactive glass/chitosan composite scaffold as hemostatic agents, ACS applied materials & interfaces, 9 (2017) 31381-31392.
[49] A. Moghanian, R. Portillo-Lara, E. Shirzaei Sani, H. Konisky, S.H. Bassir, N. Annabi, Synthesis and characterization of osteoinductive visible light-activated adhesive composites with antimicrobial properties, Journal of tissue engineering and regenerative medicine, 14 (2020) 66-81.
[50] Y.-F. Goh, A.Z. Alshemary, M. Akram, M.R.A. Kadir, R. Hussain, *In vitro* characterization of antibacterial bioactive glass containing ceria, Ceramics International, 40 (2014) 729-737.
[51] M. Gholipourmalekabadi, M. Sameni, A. Hashemi, F. Zamani, A. Rostami, M. Mozafari, Silver-and fluoride-containing mesoporous bioactive glasses versus commonly used antibiotics: Activity against

multidrug-resistant bacterial strains isolated from patients with burns, Burns, 42 (2016) 131-140.
[52] C. Wu, Y. Zhou, M. Xu, P. Han, L. Chen, J. Chang, Y. Xiao, Copper-containing mesoporous bioactive glass scaffolds with multifunctional properties of angiogenesis capacity, osteostimulation and antibacterial activity, Biomaterials, 34 (2013) 422-433.
[53] P. Chavoshnejad, M.J. Razavi, Effect of the Interfiber Bonding on the Mechanical Behavior of Electrospun Fibrous Mats, Scientific Reports, 10 (2020) 1-10.
[54] K.K. Balan, V. Sivanesan, N. Moorthy, D. Budhhan, S. Jeyaseelan, S. Sundaramoorthy, Effect of thickness of mat and testing parameters on tensile strength variability of electrospun nanofibrous mat, Materials Today: Proceedings, 3 (2016) 1320-1329.
[55] J. Jordan, K.I. Jacob, R. Tannenbaum, M.A. Sharaf, I. Jasiuk, Experimental trends in polymer nanocomposites—a review, Materials science and engineering: A, 393 (2005) 1-11.
[56] T. Suchý, M. Šupová, M. Bartoš, R. Sedláček, M. Piola, M. Soncini, G.B. Fiore, P. Sauerová, M.H. Kalbáčová, Dry versus hydrated collagen scaffolds: are dry states representative of hydrated states?, Journal of Materials Science: Materials in Medicine, 29 (2018) 20.
[57] A. Saatchi, A.R. Arani, A. Moghanian, M. Mozafari, Synthesis and characterization of electrospun cerium-doped bioactive glass/chitosan/polyethylene oxide composite scaffolds for tissue engineering applications, Ceramics International, (2020).
[58] C.E.G. Garcia, F.A.S. Martínez, F. Bossard, M. Rinaudo, Biomaterials based on electrospun chitosan. Relation between processing conditions and mechanical properties, Polymers, 10 (2018) 257.
[59] P. Sangsanoh, P. Supaphol, Stability improvement of electrospun chitosan nanofibrous membranes in neutral or weak basic aqueous solutions, Biomacromolecules, 7 (2006) 2710-2714.
[60] S. Mengistu Lemma, F. Bossard, M. Rinaudo, Preparation of pure and stable chitosan nanofibers by electrospinning in the presence of poly (ethylene oxide), International journal of molecular sciences, 17 (2016) 1790.
[61] P. Bösiger, I.M. Richard, L. Le Gat, B. Michen, M. Schubert, R.M. Rossi, G. Fortunato, Application of response surface methodology to tailor the surface chemistry of electrospun chitosan-poly (ethylene oxide) fibers, Carbohydrate polymers, 186 (2018) 122-131.
[62] A.N. Sohi, H. Naderi-Manesh, M. Soleimani, S. Mirzaei, M. Delbari, M. Dodel, Influence of chitosan molecular weight and poly (ethylene oxide): Chitosan proportion on fabrication of chitosan based electrospun nanofibers, Polymer Science, Series A, 60 (2018) 471-482.
[63] B.K. Gu, S.J. Park, M.S. Kim, C.M. Kang, J.-I. Kim, C.-H. Kim, Fabrication of sonicated chitosan nanofiber mat with enlarged porosity for use as hemostatic materials, Carbohydrate Polymers, 97 (2013) 65-73.
[64] D. Kozon, K. Zheng, E. Boccardi, Y. Liu, L. Liverani, A.R. Boccaccini, Synthesis of monodispersed Ag-doped bioactive glass nanoparticles via surface modification, Materials, 9 (2016) 225.